

# Unlocking the molecular secrets of sodium-coupled transporters

Harini Krishnamurthy<sup>1</sup>, Chayne L. Piscitelli<sup>1,2</sup> & Eric Gouaux<sup>1,3</sup>

**Transmembrane sodium-ion gradients provide energy that can be harnessed by 'secondary transporters' to drive the translocation of solute molecules into a cell. Decades of study have shown that such sodium-coupled transporters are involved in many physiological processes, making them targets for the treatment of numerous diseases. Within the past year, crystal structures of several sodium-coupled transporters from different families have been reported, showing a remarkable structural conservation between functionally unrelated transporters. These atomic-resolution structures are revealing the mechanism of the sodium-coupled transport of solutes across cellular membranes.**

A multitude of transmembrane transporter proteins have evolved to catalyse the movement of small polar or charged molecules across the hydrophobic barrier of the membrane bilayer<sup>1</sup>. A large class of these proteins, termed secondary transporters, use the discharge of an ionic gradient to power the 'uphill' translocation of solute molecules across membranes. By coupling solute movement to ion transport, secondary transporters are able to concentrate solutes across a membrane by a factor of  $10^6$  (ref. 2), and solute flux can occur  $10^5$  times faster than by simple passive diffusion<sup>3,4</sup>.

Secondary transporters are found in all species throughout the kingdoms of life<sup>5</sup>. In humans, they participate in a range of physiological processes, from the uptake of nutrients in the intestine<sup>6</sup> to the transport of  $\text{Na}^+$  and  $\text{Cl}^-$  in the kidney<sup>7</sup> and the removal of neurotransmitters from the synaptic cleft<sup>8</sup>. Secondary transporters are therefore the target of multiple therapeutic agents, including thiazide diuretics, which inhibit a  $\text{Na}^+/\text{Cl}^-$  symporter in the distal convoluted tubule of the kidney<sup>9</sup>, and selective serotonin re-uptake inhibitors (antidepressants), which block the activity of the serotonin transporter<sup>10</sup>.

At the level of primary structure, analyses of amino-acid sequence suggest that there are more than 100 distinct families of secondary transporter<sup>11</sup>, with more than 40 families identified in humans alone<sup>12</sup>. With respect to biological function, these amino-acid sequences encode transporters that act on a range of substrates including elemental cations and anions, aromatic neurotransmitters, nutrients and di- and tripeptides<sup>13,14</sup>. Transport is usually driven by proton or sodium transmembrane gradients<sup>12,13</sup>.

In this Review, we focus on transporters that are coupled to sodium ions. We will discuss what recent crystallographic advances relating to sodium-coupled transporters can tell us about the coupling of substrates to ions, the conformational state of the transporter at different stages of the transport cycle, the mechanisms of transport inhibition, and how the substrate and ion pathway is alternately opened and closed — or gated — to maintain a tightly coupled transport mechanism.

## Alternating-access mechanism

The mechanism by which secondary transporters couple the chemical potential of an ionic gradient to the translocation of solute has been debated for decades. Peter Mitchell provided early insights into the

mechanism of secondary transporters by suggesting that they occupy two alternating structural states: one in which the substrate-binding pocket is accessible to extracellular solution ('open-to-out'), and another in which the binding pocket is accessible to the cytoplasm ('open-to-in')<sup>15</sup>. In this simple model, coupled transport occurs by the synergistic binding of substrate and ion to the open-to-out state followed by isomerization of the transporter to the open-to-in state, allowing the release of both substrate and ion to the cytoplasm<sup>16</sup>. In the late 1950s and 1960s, the basic idea of a two-state alternating-access mechanism was recast in several forms, from the 'gate-type non-carrier' mechanism of Clifford Patlak<sup>17</sup> to the two-state 'allosteric model' of George Vidaver<sup>18</sup> and the 'alternating access' model of Oleg Jardetzky<sup>19</sup>.

Molecular mechanisms of secondary transporters based on atomic structures did not emerge until almost 40 years later, largely because these transporters are hydrophobic and dynamic, making them difficult to crystallize. In 2002, the first crystal structure of a secondary transporter was reported<sup>20</sup>, the proton-driven multidrug efflux pump AcrB of the resistance nodulation cell division (RND) family from *Escherichia coli*. In 2003, the crystal structures of two major facilitator superfamily (MFS) transporters were solved: the glycerol-3-phosphate/phosphate antiporter GltP<sup>21</sup> and the proton-coupled lactose symporter LacY<sup>22</sup>. Even though AcrB has a markedly different fold from the MFS transporters, each of these structures revealed an internal two-fold structural pseudo-symmetry that relates the amino-terminal half of the transporter to the carboxy-terminal half by an axis running through the centre of the transporter, approximately perpendicular to the membrane. Furthermore, the outward-facing conformations adopted by GltP and LacY suggest that the transport mechanism involves a 'rocker switch' motion of the two symmetry-related halves, alternately opening and closing 'gates' to the extracellular and intracellular solutions.

The first atomic-resolution structural insights into the mechanisms of sodium-coupled secondary transporters were reported in 2004 and 2005 with the structures of the aspartate transporter GltPh<sup>23</sup> of the dicarboxylate/amino-acid:cation symporter (DAACS) family, followed by the  $\text{Na}^+/\text{H}^+$  antiporter NhaA from *E. coli*<sup>24</sup> and the bacterial leucine transporter LeuT<sup>25</sup> of the neurotransmitter:sodium symporter (NSS) family. The structures of GltPh, NhaA and LeuT not only revealed unique membrane protein folds but also reinforced the theme of internal two-fold

<sup>1</sup>Vollum Institute, <sup>2</sup>Department of Biochemistry and Molecular Biology, and <sup>3</sup>Howard Hughes Medical Institute, Oregon Health and Science University, 3181 SW Sam Jackson Park Road, Oregon 97239, USA.

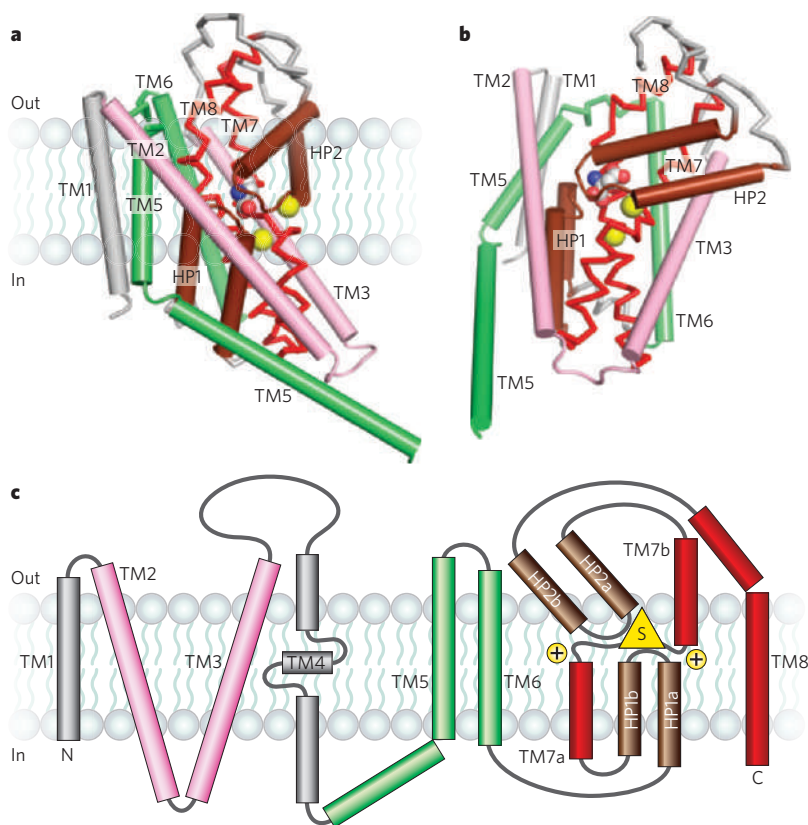


**Figure 1 | Architecture of the GltPh fold.** **a**, The core transmembrane helices of GltPh are shown, illustrating how the first six transmembrane segments surround the elements of the transporter machinery. The inverted cradle formed by TM2/TM3 and TM5/TM6 is coloured pink and green, respectively. The re-entrant hairpins (HP1 and HP2) are shown in brown and the partly unwound TM7 and the amphipathic TM8 are shown in red. The view is parallel to the membrane and only one subunit of the GltPh trimer is shown. TM4 is omitted for clarity **b**, The same elements as **a** viewed approximately perpendicular to the membrane. The bound substrates (carbon, grey; oxygen, red; nitrogen, blue) and sodium ions (yellow) are shown. **c**, Topology diagram for GltPh with substrate and ions depicted as yellow triangle and circles, respectively.

structural symmetry and discontinuous transmembrane helices<sup>26</sup>.

GltPh, which assembles as a homotrimer, displays a pseudo-two-fold symmetrical relationship between crucial elements of the protomer architecture, including two re-entrant hairpin loops (HP1 and HP2), together with the transmembrane helix TM7a and the first half of TM8 (ref. 23). The relevance of the two-fold axis to the transporter mechanism is particularly striking, and it suggests that HP1 and HP2 may undergo alternating, symmetry-related motions that open and close access to the substrate- and ion-binding sites<sup>23</sup> (Fig. 1).

In LeuT, which has a different fold from GltPh, an internal two-fold pseudo-symmetry axis, running parallel to the membrane plane through the centre of the transporter, relates the first five transmembrane helices (TM1–TM5) to the second five helices (TM6–TM10)<sup>25</sup> (Fig. 2). Surprisingly, the fold seen in LeuT was also observed in the subsequently reported structure of the galactose transporter vSGLT of the solute:sodium symporter (SSS) family<sup>27</sup>, and in the benzyl-hydantoin transporter Mhp1 of the nucleobase:cation symporter (NCS1) family<sup>28</sup>. Both vSGLT (ref. 27) and Mhp1 (ref. 28) contain the ‘5+5’ inverted structural symmetry motif defined by TM1–TM10 of LeuT, even though these three transporters do not share significant amino-acid sequence identity or have the same number of transmembrane segments. In vSGLT, which has 14 transmembrane helices compared with 12 in LeuT and Mhp1, an N-terminal transmembrane helix precedes the 5+5 helix repeat and three additional helices follow the repeat. That different transporters have the same common helix core but have additional transmembrane segments on the periphery supports the idea that the two-fold-related 5+5 transmembrane repeat defines the fundamental machinery of these transporters.

Not only have the crystal structures of vSGLT, LeuT and Mhp1 effectively ‘collapsed’ the SSS<sup>29</sup>, NSS<sup>30</sup> and NCS1 transporter families into one structural group, they also suggest that other secondary transporters, previously believed to belong to distinct families, may also have LeuT-like folds. The similarity in architecture among LeuT, vSGLT and Mhp1 further implies commonalities in mechanism, ranging from the principles of substrate and ion binding and specificity to conformational changes associated with transport. Atomic models of these functionally disparate

yet structurally related transporter families have provided insight into the principles of sodium-coupled transport, and are beginning to clarify an alternating-access mechanism that is distinctly different from that of the MFS family. Conversely, comparison of the structurally disparate LeuT and GltPh transporters suggest commonalities in the concept of ‘gates’, how they function in the alternating-access mechanism, and in the mechanism of competitive inhibition.

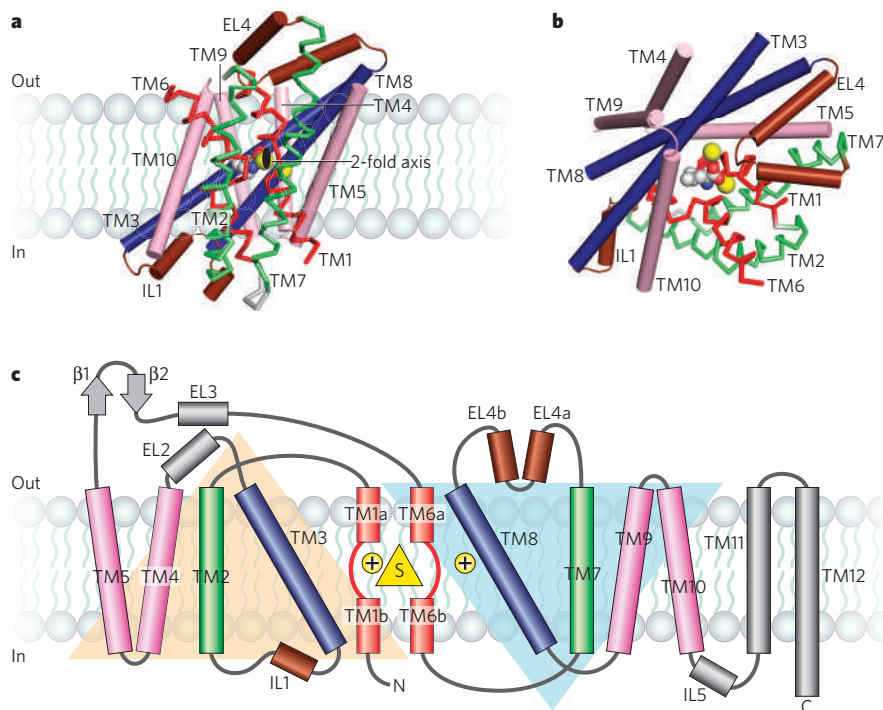
### A central pathway inside a scaffold

Close inspection of the LeuT, vSGLT and Mhp1 structures (Fig. 2) shows that the 5+5 transmembrane motif consists of two interior pairs of symmetry-related helices — TM1 and TM6, and TM3 and TM8 — that are nested within an outer ring of helices, TM2, TM4, TM5, TM7, TM9 and TM10 (numbered according to LeuT). Consistent with mutagenesis and functional studies<sup>31–34</sup>, these interior pairs largely define the central translocation pathway that contains the binding sites for substrate and ions. The three structures show that the substrate-binding site lies in the centre of the interior pairs, and coincides with the internal two-fold symmetry axis.

Among the outer ring of helices, symmetry-related TM4 and TM5, and TM9 and TM10, form inverted V-shaped pincers that cradle the interior pair of TM3 and TM8, whereas TM2 and TM7, also related by the two-fold axis of symmetry, link TM1 and TM6 with the intracellular and extracellular helix–loop–helix structures, IL1 and EL4. We suggest that the outer ring of helices, which nestles around the interior pairs, provides a framework to stabilize the transporter within the lipid membrane, and that it couples conformational changes on one side of the membrane to movements on the other side.

The central translocation pathway surrounded by a protein scaffold is also observed in the GltPh fold (Fig. 1). In GltPh, the transport machinery of HP1, HP2, TM7 and TM8, forming a C-terminal domain, is enveloped by a ring of six transmembrane helices from the N-terminal domain of the transporter. In this case, the crucial role of the C-terminal domain in defining the transport pathway was suggested by studies showing that functionally important residues were localized to the C terminus, and that the C-terminal domain was more highly con-

**Figure 2 | Architecture of the LeuT fold.** **a**, View of the core 5+5 repeat structure for LeuT showing the inverted scaffold of TM4, TM5, TM9 and TM10 holding the long bracing helices of TM3 and TM8 and the jointed, finger-like and partly unwound TM1 and TM6 helices. Bracing TM1 and TM6 are TM2 and TM7 (green). Re-entrant, pseudo-two-fold related loops that either partly (EL4) or fully (IL1) occlude central binding sites are shown in brown. View is parallel to the membrane. **b**, The same elements as in **a** viewed approximately perpendicular to the membrane. The bound substrate (carbon, grey; oxygen, red; nitrogen, blue) and sodium ions (yellow) are shown. **c**, Topology diagram for LeuT with substrate and ions depicted as yellow triangle and yellow circles, respectively. The large beige and blue triangles overlap the five helix repeats related by the pseudo-two-fold axis of symmetry.



served than the N-terminal one<sup>35–37</sup>. For GltPh and its orthologues, the scaffold of TM1–TM6 not only supports elements of the transport pathway, but also mediates essential intersubunit contacts in the trimer.

### Substrate- and ion-binding sites

LeuT has a single substrate-binding site at its centre, surrounded by the interior helices, TM1, TM3, TM6 and TM8 (ref. 25). The binding sites for galactose in vSGLT<sup>27</sup> and benzyl-hydantoin in Mhp1<sup>28</sup> are also similarly located (Fig. 3a). Directly adjacent to the primary binding site, TM1 and TM6 in LeuT and Mhp1, or TM2 and TM7 in vSGLT, have interruptions in their helical conformations, a structural feature seen in other membrane proteins that transport ions<sup>24,38,39</sup>. The

interruption in the  $\alpha$ -helical structures in the proximity of the binding site exposes main-chain hydrogen-bonding partners and orients the helical dipoles to create a polar environment for coordinating substrate and ions within the lipid bilayer<sup>25</sup>. These electrostatic elements, together with side-chain atoms, sculpt the steric, chemical and electrical properties of the binding pocket, conferring on a given transporter selectivity for a substrate based on its size, polarity and charge<sup>40</sup>.

Recent ligand-binding experiments and steered-molecular-dynamics simulations of LeuT have suggested that there is an additional secondary binding site between the primary site and the bulk extracellular solution, located near R30 and D404 (refs 41, 42). It has been proposed<sup>41</sup> that the simultaneous occupancy of this secondary site triggers the

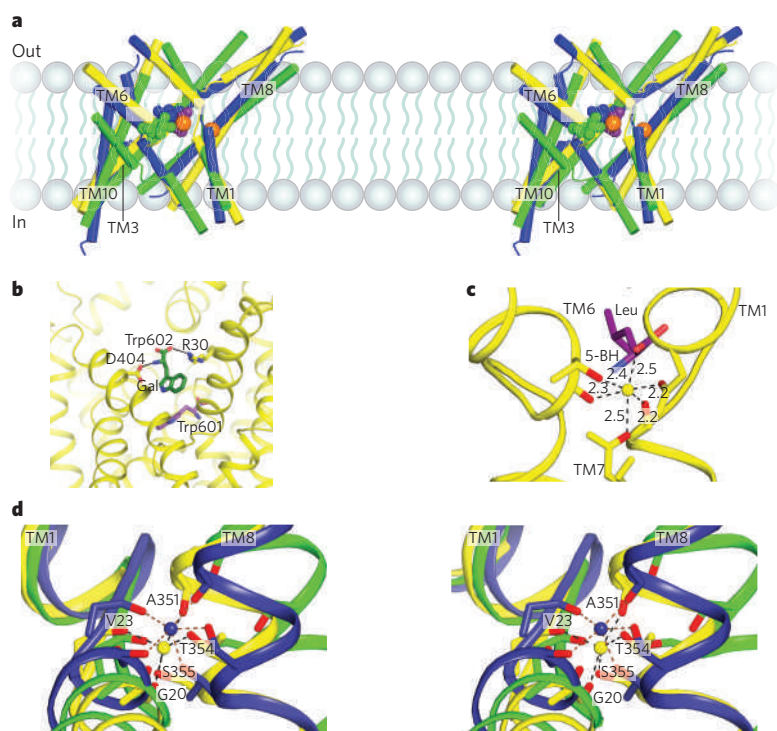


**Figure 3 | Conserved substrate- and ion-binding sites in LeuT, vSGLT and Mhp1.** **a**, Stereo diagram of the superpositioned occluded structures of LeuT (yellow), Mhp1 (blue) and vSGLT (green) showing the location of their primary substrate-binding sites roughly in the middle of the membrane bilayer and close to the discontinuous regions of TM1 and TM6. Substrate (Gal, galactose (green); 5-BH, 5-benzyl hydantoin (blue); Leu, leucine (purple) and LeuT Na<sup>+</sup> ions (orange) are shown. For clarity, only TM1, TM3, TM6, TM8 and TM10 are shown. **b**, View of the secondary binding site in LeuT. A second Trp molecule, Trp 602, is bound between R30 and D404 in the open-to-out conformation stabilized by Trp 601 in the primary binding site. **c**, The sodium ion (yellow sphere) at the Na1 site in LeuT is octahedrally coordinated by residues from TM1, TM6 and TM7 as well as bound leucine (purple). Distances in Å are shown. **d**, Stereo representation of superpositioned LeuT (yellow), vSGLT (green) and Mhp1 (blue) structures shows the location of their Na2 binding sites. The sodium ions at the Na2 site of LeuT and Mhp1 are shown as yellow and blue spheres, respectively. Residues contributing side-chain and main-chain oxygens that coordinate the sodium ions are shown as sticks with LeuT residues (A351, T354, S355, G20 and V23) labelled.

**Table 1 | Families of sodium-coupled transporters grouped according to structural fold**

Structural fold	Family	Transporter	Transported solute	Co-transported ions	
LeuT fold	NSS (SLC6)	<i>LeuT</i>	Amino acids	2Na <sup>+</sup>	
		TyT1	Tyrosine	2Na <sup>+</sup>	
		TnaT	Tryptophan	2Na <sup>+</sup>	
		CAATCH1	Neutral amino acids	2Na <sup>+</sup> or 2K <sup>+</sup>	
		CRT	Creatine	2Na <sup>+</sup> , 1Cl <sup>-</sup>	
		GlyT1c	Glycine	2Na <sup>+</sup> , 1Cl <sup>-</sup>	
		GlyT2b	Glycine	3Na <sup>+</sup> , 1Cl <sup>-</sup>	
		NET	Noradrenaline	1Na <sup>+</sup>	
		GAT-1	γ-Aminobutyric acid	2Na <sup>+</sup> , 1Cl <sup>-</sup>	
		SERT	Serotonin	1Na <sup>+</sup> , 1Cl <sup>-</sup> , 1K <sup>+</sup>	
	DAT	Dopamine	2Na <sup>+</sup>		
	B <sup>0,+</sup>	Neutral and cationic amino acids	2Na <sup>+</sup> , 1Cl <sup>-</sup>		
	SSS (SLC5)	<i>vSGLT</i>	Glucose/galactose	1Na <sup>+</sup>	
		PutP	Proline	1Na <sup>+</sup>	
		NIS	Iodide	2Na <sup>+</sup>	
		PanF	Pantothenate	1Na <sup>+</sup>	
		SMCT	Monocarboxylate	3Na <sup>+</sup>	
		SMIT2	Myoinositol	2Na <sup>+</sup>	
		NCS1	<i>Mhp1</i>	Hydantoin	1Na <sup>+</sup>
			CodB	Cytosine	1H <sup>+</sup>
Nrt1			Nicotinamide riboside	1H <sup>+</sup>	
Thi10			Thiamine	1H <sup>+</sup>	
Tpn1	Vitamin B6	1H <sup>+</sup>			
GltPh fold	DAACS (SLC1)	<i>GltPh</i>	Aspartate	1Na <sup>+</sup>	
		DctA	C4-dicarboxylate	2H <sup>+</sup>	
		EAAT 1-5	Glutamate/aspartate	3Na <sup>+</sup> , 1H <sup>+</sup> , 1K <sup>+</sup>	
		AscT1	Neutral amino acids	1Na <sup>+</sup>	
		System B <sup>0</sup>	Broad-specificity amino acids	1Na <sup>+</sup>	
NhaA fold	NhaA	<i>NhaA</i>	Sodium ion	2H <sup>+</sup>	

Families of sodium-coupled transporters (for classification see [www.tcdb.org](http://www.tcdb.org))<sup>44</sup> are grouped into the three known structural folds. Where applicable, the SLC class<sup>52</sup> is indicated in parenthesis. The name of each fold is based on the first transporter structure solved that has that fold. Representative transporters from each family are listed, and ion stoichiometry is indicated in the 'Co-transported ions' column when supported by biochemical data ([www.tcdb.org](http://www.tcdb.org))<sup>44</sup>. Transporters for which crystal structures have been determined are italicized. Some of the transporters are H<sup>+</sup> rather than Na<sup>+</sup> dependent.

intracellular release of substrate and sodium ions from the primary site. X-ray diffraction studies of LeuT, by contrast, do not show binding of either the substrate leucine or the substrate analogue selenomethionine anywhere other than the primary binding site<sup>40</sup>. However, LeuT complexed with tryptophan, which locks the transporter in an open-to-out conformation, does bind a second tryptophan molecule (Trp 602) between R30 and D404 (ref. 40) (Fig. 3b). We suggest that this site is transiently occupied as substrates move from the extracellular vestibule to the primary binding site when the transporter is in the open-to-out conformation.

The high-resolution structure of LeuT also identified the presence of two Na<sup>+</sup> binding sites, which we label as Na1 and Na2 (ref. 25). The sodium ion at the Na1 site is octahedrally coordinated by five protein ligands and the carboxylate of the substrate leucine (Fig. 3c), demonstrating that ion and substrate binding are directly coupled. By contrast, the Na2 site is located roughly 6 Å away from the substrate in LeuT and the sodium ion at this site is bound with a trigonal bipyramidal coordination geometry (Fig. 3d). Intriguingly, by structural comparison, a sodium-ion binding site similar to the Na2 site in LeuT has been identified in both *vSGLT* and *Mhp1*, positioned about 10 Å away from the substrates<sup>27,28</sup>. Although the resolutions of the *vSGLT* and *Mhp1* structures are not high enough to unambiguously assign a sodium ion to the site, a sodium ion at this position in *vSGLT* is supported by biochemical and mutagenesis studies on *vSGLT* and other SSS family members, including the sodium/iodide symporter<sup>27,43,44</sup>. These observations indicate a role for an ion bound at the Na2 site not only in substrate binding, but also in conformational changes associated with substrate transport. Studies on GAT1 (ref. 45), as well as

molecular-dynamic and free-energy simulations of LeuT<sup>46</sup>, suggest that the Na2 site is a low-affinity site that can readily give up its ion to the bulk phase, promoting release of the substrate<sup>47</sup>.

Sodium-to-substrate stoichiometry varies not only between sodium-coupled transporters, but also between members of the same family, depending on the thermodynamic driving force required for substrate uptake<sup>4</sup>. The requirement for transport varies from one to three sodium ions per substrate in the NSS<sup>2,48–50</sup> and SSS families<sup>44,51–53</sup> (Table 1). Because *vSGLT* and *Mhp1* probably have a sodium-ion binding site similar to the LeuT Na2 site, we suggest that this is a common ion site for divergent transporters and is essential for coupled substrate binding and symport. Although the Na1 site is less conserved among these transporters from different families, a sodium ion bound at this site not only enhances substrate binding for members of the NSS family, but also provides favourable interactions with the co-transported chloride ion<sup>54,55</sup>. Some LeuT orthologues couple substrate transport to three sodium ions, but there is no direct experimental evidence for the location of a third sodium-ion binding site<sup>4</sup>.

### Conformational states

The crystal structures of LeuT<sup>25,40,56</sup>, *Mhp1* (ref. 28), *vSGLT*<sup>27</sup> and *GltPh*<sup>23,57</sup> provide evidence for the conformations of sodium-coupled secondary transporters as they proceed through the transport cycle. These structures are consistent with a mechanism of transport (Fig. 4a) in which an outward-facing conformation of the transporter (T<sup>out</sup>) binds substrate and ions and subsequently isomerizes to an inward-facing conformation (T<sup>in</sup>), via substrate- and ion-bound intermediate states (T<sup>M<sup>in</sup></sup> and T<sup>M<sup>out</sup></sup>) analogous to enzyme–substrate Michaelis complexes. After

the release of the substrate and ions, the  $T^{\text{in}}$  state recycles back to the  $T^{\text{out}}$  state, either in the apo form (without a bound substrate), through a potassium-bound state (as is the case for glutamate<sup>58</sup> and serotonin transporters<sup>59</sup>), or back through a  $T^{\text{MS}}$  state (with substrate exchange).

One observation from the crystallographic studies is the presence of a stable occluded state for the substrate- and ion-bound ternary complex of each of the four transporters (Fig. 4a). This state is characterized by the bound substrate residing in a closed or partly occluded binding pocket, where dissociation from the pocket would require a conformational change. Despite the common steric occlusion of the substrate, the degree to which the four transporters block solvent accessibility to the binding pocket from the extracellular and cytoplasmic sides varies (Fig. 4a).

In the substrate-bound state of Mhp1 and LeuT, the occluded state has an outward-facing conformation ( $T^{\text{MSout}}$ ), with the extracellular pathway being kept open to solvent. In LeuT, the extracellular solvent-exposed region is formed by a large hydrophobic vestibule. At the base of this vestibule are two highly conserved residues, Tyr 108 and Phe 253, which close the top of the binding pocket, creating an occluded substrate-binding site. In Mhp1, the structural elements that occlude the substrate benzyl-hydantoin are different from those of LeuT and involve the N-terminal half of TM10. GltPh also has an outward-facing occluded conformation (Fig. 4a). Aspartate is bound between the tips of the HP1 and HP2 loops, which are closed over the binding site like lids, preventing the dissociation of substrate to either side of the transporter.

In contrast to LeuT and Mhp1, the occluded state of vSGLT adopts an inward-facing conformation ( $T^{\text{MSin}}$ ), exposing a cavity to intracellular

solution (Fig. 4a), consistent with accessibility studies carried out on PutP<sup>43</sup> and SERT<sup>60–63</sup>, orthologues of vSGLT and LeuT, respectively. Akin to leucine binding in LeuT, galactose is bound to vSGLT in a central binding pocket located above the intracellular vestibule, and is occluded from the vestibule by a conserved aromatic residue, Tyr 263. The inward-facing, occluded conformation of galactose-bound vSGLT is structurally different from that observed for substrate-bound LeuT or Mhp1, but there is a simple relationship between the two distinct states: the outward- and inward-facing states are related by the common two-fold axis of internal symmetry that relates the 5+5 transmembrane repeats, suggesting that the symmetrical relationship between LeuT and vSGLT approximates the mechanistic relationship between the  $T^{\text{MSin}}$  and  $T^{\text{MSout}}$  states.

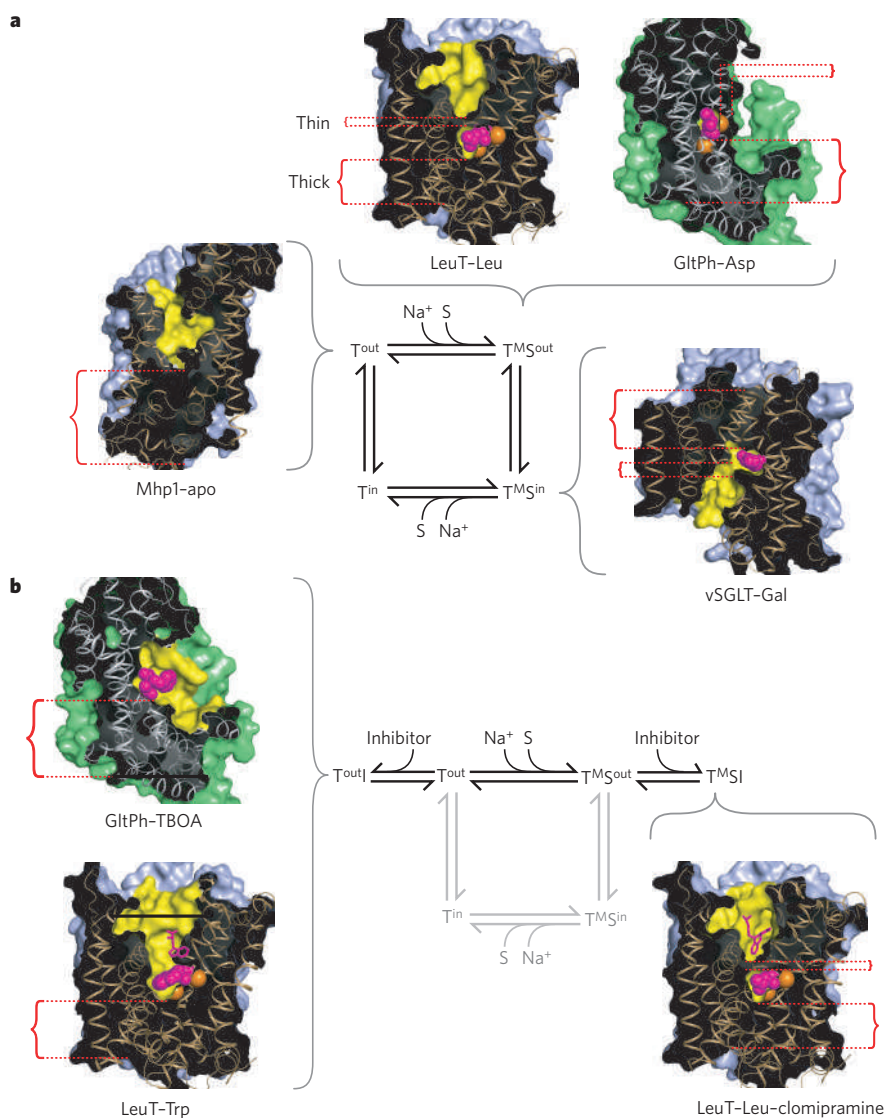
The crystal structure of Mhp1 in the unliganded form shows an open-to-out conformation representing the  $T^{\text{out}}$  state of the transport cycle (Fig. 4a). Comparison of the ligand-bound occluded form of Mhp1 with the apo open-to-out state shows that the N-terminal half of TM10 bends inwards in response to ligand binding to form the occluded state. Further insight into the conformation of the  $T^{\text{out}}$  state comes from the crystal structures of LeuT and GltPh bound to competitive inhibitors that trap the open-to-out conformations of the transporters<sup>40,57</sup> (Fig. 4b).

### Mechanisms of inhibition

The crystal structures of LeuT bound to competitive and non-competitive inhibitors have afforded us a glimpse into the mechanisms of inhibition for the NSS family of transporters. In 2007, crystal structures of LeuT bound to the tricyclic antidepressants (TCAs) clomipramine,

**Figure 4 | Crystal structures of transport intermediates.**

**a**, Transport cycle based on an alternating-access-type mechanism together with insights from crystallographic studies. Clockwise from the  $T^{\text{out}}$  state: Mhp1–apo (PDB code 2JLN), LeuT–Leu (PDB code 2A65), GltPh–Asp (PDB code 2NWX) and vSGLT–Gal (PDB code 3DH4). **b**, The inhibitory branches of the transport cycle from **a**. On the left, structures of GltPh–TBOA (PDB code 2NWW) and LeuT–Trp (PDB code 3F3A) represent an open-to-out competitive inhibitor-bound state. On the right, the structure of LeuT–Leu–clomipramine (PDB code 2Q6H) represents a non-competitive inhibitor-bound occluded state. Cross-sectional illustrations of the crystal structures of each transporter are shown associated with the states of the cycle they represent. The positions of the ‘thin’ gates and ‘thick’ gates are highlighted by red dashed lines. The solvent-accessible surface area, calculated with a probe radius of 1.4 Å, is shown in light blue for the LeuT-fold structures and green for GltPh-fold structures. Yellow regions highlight the surfaces of the binding site and cavities that penetrate the structures. Bound ligands, shown as van der Waals spheres, are coloured magenta, with sodium ions in orange. The view of each transporter is approximately parallel to the membrane plane, with the extracellular side at the top of each figure. PDB, Protein Data Bank; TBOA, aspartate analogue.



desipramine and imipramine were reported<sup>56,64</sup>. These molecules have therapeutic value as competitive inhibitors of the human serotonin transporter<sup>65</sup> and block re-uptake of serotonin from synapses, thereby prolonging activation of the serotonin receptor. For LeuT, however, the mechanism of inhibition by TCAs is non-competitive<sup>56</sup>. The structures of the LeuT–TCA complexes reveal that the TCA molecule binds in the outward-facing vestibule, a partly hydrophobic cavity that binds other non-polar molecules, including *n*-octyl- $\beta$ -D-glucopyranoside<sup>40</sup>. The TCA is situated directly above the R30–D404 salt bridge, where the guanidinium head group of the arginine has flipped to form a salt bridge with the aspartate, stabilizing the occluded state of LeuT ( $T^{M_{SI}}$ ; Fig. 4b), and preventing the further conformational changes needed for progress around the transport cycle. The identification of this inhibitory allosteric site is consistent with a general mechanism of non-competitive inhibition in which the substrate-binding site and inhibitor site do not overlap, trapping the transporter in an inactive

state. The non-competitive mechanism for the inhibition of LeuT by TCAs is different from the competitive mechanism for the inhibition of SERT by TCAs<sup>65</sup>. Nevertheless, the structural principles revealed by the LeuT–TCA complexes define a mechanism of allosteric inhibition in NSS family transporters and, by extension, in other transporters with the LeuT fold.

The structural basis for competitive inhibition was recently revealed by the crystal structure of LeuT bound to tryptophan<sup>40</sup>. Tryptophan acts as a strut, where the bulky indole ring is wedged into the binding pocket, displacing the  $\alpha$ -amino and  $\alpha$ -carboxylate moieties outwards by about 2 Å relative to their positions in the leucine-bound occluded state. There is insufficient space to fully accommodate the indole ring in the substrate-binding pocket, so the transporter is effectively propped open by interactions of the inhibitor's  $\alpha$ -substituents with TM1b and TM6a, and of the indole ring with TM3, TM8 and TM10. In this way, the transporter is locked open ( $T^{M_{SI}}$ ; Fig. 4b) and blocked from progressing to the occluded  $T^{M_{S^{out}}}$  state of the transport cycle.

The crystal structure of GltPh bound to the competitive inhibitor TBOA, a bulky aspartate analogue, reveals a similar principle of competitive inhibition for transporters with the GltPh fold<sup>57</sup> (Fig. 4b). The aspartate group of TBOA binds in a similar position as the substrate L-aspartate, lodged between TM7, TM8 and HP1. However, the large benzyl moiety of TBOA sticks out towards HP2, propping HP2 in an open conformation (Fig. 4b), disrupting sodium site 2 and precluding the formation of the occluded state.

The observation that bulky substrate analogues act as competitive inhibitors of transport to stabilize an opening of the extracellular side of the transporter is supported by substituted cysteine accessibility method (SCAM) assays for the eukaryotic NSS homologue GAT1, as well as the human glucose transporter hSGLT, a member of the SSS family<sup>66</sup>. The consistency of these results with the LeuT–Trp crystal structure suggests that the mechanism of inhibition is likely to be similar for other sodium-coupled transporters that share the LeuT fold, and that a comparable principle seems to be found in other families of structurally disparate transporters, such as those adopting the GltPh fold.

### Permeation pathways and gating mechanisms

In transporters with the GltPh fold (GltPh) and the LeuT fold (LeuT, vSGLT and Mhp1), the primary substrate- and ion-binding sites are flanked by two gates, one controlling access to the outside of the cell, the other controlling access to the inside. Only one of these gates can open at a time, allowing substrates and ions to reach the primary binding sites without opening up a continuous transmembrane pore. Understanding how secondary transporters work is fundamentally a question of how the gates work: what principles govern the coordinated, alternate opening and closing of the extracellular and intracellular gates when substrates bind on the outside and unbind on the inside. To answer this question, we must consider the conformational changes that occur during transport and the likely pathways that substrates and ions take when they bind to, and unbind from, their primary sites.

In the small group of sodium-coupled transporter structures, for a given transporter trapped in a specific state, the gates that control access to and from the primary binding site are often asymmetric, with the extracellular gate being less substantial or 'thinner' than the cytoplasmic gate, or vice versa (Fig. 4a). This is observed for transporters with the GltPh fold as well as those with the LeuT fold. For example, in the outward-facing occluded leucine-bound LeuT complex, only a few residues directly block access from the primary binding site (Tyr 108 and Phe 253), forming a 'thin' gate at the base of a solvent-filled cavity to the outside. By contrast, the cytoplasmic 'thick' gate is made up of about 20 Å of packed protein, including TM1a, TM3, TM6b, TM8 and TM10, along with the N terminus and IL1 (Fig. 5a, c, e). Similarly, in the substrate-bound state of GltPh, the extracellular gate is made up of just a few residues at the tip of HP2, whereas the cytoplasmic gate is composed of a roughly 15-Å slab of helices and side chains (HP1, TM7a and TM8).

The substrate- and ion-bound inward-facing occluded state of

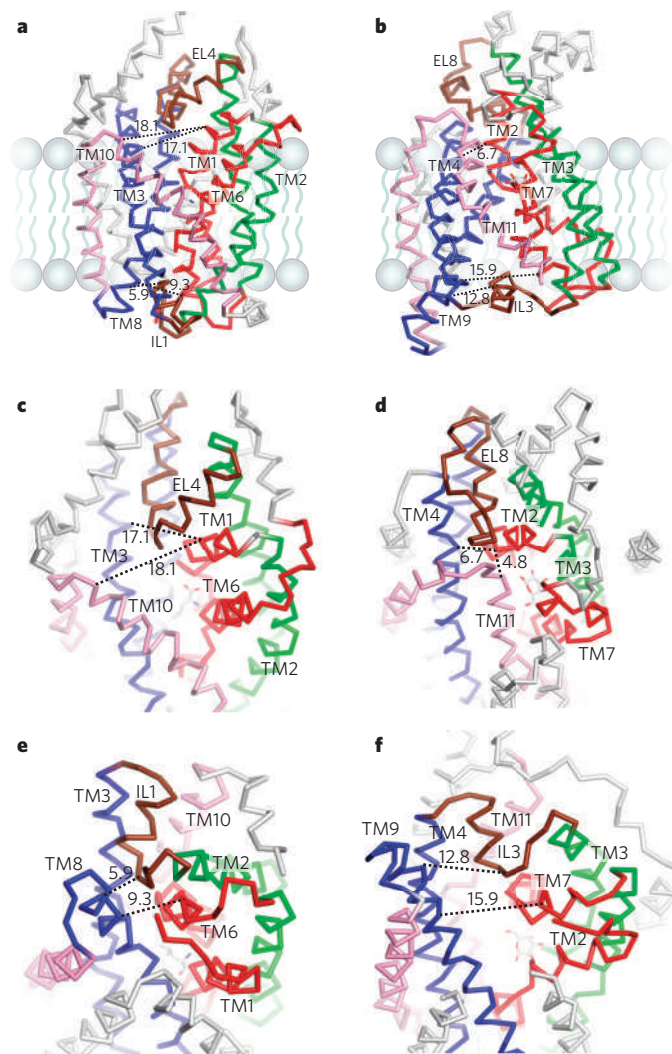


**Figure 5** | Comparative views of substrate-bound LeuT in the  $T^{M_{S^{out}}}$  state (left) and vSGLT in the  $T^{M_{S^{in}}}$  state (right). **a, b**, Views parallel to the membrane of LeuT (**a**, PDB code 2A65) and vSGLT (**b**, PDB code 3DH4). **c, d**, Top-down view of the extracellular pathway for LeuT (**c**) and vSGLT (**d**). **e, f**, Bottom-up view of the intracellular pathway for LeuT (**e**) and vSGLT (**f**). Equivalent structural elements are coloured the same in both LeuT and vSGLT. To help gauge the re-organization of the extra- and intracellular elements, black dashed lines indicate distances between structural elements, measured from structurally similar residues in the two transporters. Considering the internal two-fold symmetry, note the similar organization of the open LeuT extracellular pathway (**c**) to the open vSGLT intracellular pathway (**f**), and of the closed vSGLT extracellular pathway (**d**) to the closed LeuT intracellular pathway (**e**). PDB, Protein Data Bank.

vSGLT presents a converse situation in which a thick extracellular gate is formed by TM1b, TM3, TM6a, TM10 and EL4 (numbering as LeuT) and a thin cytoplasmic gate is composed of Tyr 262, Tyr 263 and Trp 264 (Fig. 5b, d, f). Thus, the thin gates are typically defined by the side-chain atoms of a few residues, whereas the thick gates are formed by transmembrane helices packed close together, in combination with extracellular and intracellular loops such as N termini, IL1 or EL4. A prominent observation from the structures of outward-facing LeuT and Mhp1, and inward-facing vSGLT, is that the thick gate of each transporter is related to the extracellular or intracellular pathway by the internal two-fold symmetry. In any one state, the structural components of the solvent-filled pathway are reciprocal (with respect to the axis of the two-fold symmetry) to those of the thick gates.

Insight into how the thin gate opens and closes is provided by the structures of LeuT, Mhp1 and GltPh captured in both open-to-out ( $T^{\text{out}}$ ) and outward-facing occluded ( $T^{\text{M}^{\text{out}}}$ ) conformations. These structures demonstrate that substrate and ion binding results in relatively small conformational changes. In GltPh, for example, aspartate binding allows HP2 to close over the binding site, whereas TBOA binding holds it open, suggesting that the simple 'flipping' movement of HP2 primarily describes the motion of the thin gate that occludes the binding site during transport. With LeuT, in comparing the open-to-out conformation of the Trp complex with the occluded Leu-bound state, the most substantial change is the rotation of a subdomain of the transporter composed of TM1b, TM2a, TM6b and EL4, which, together with rotations of several side chains, collectively moves inwards to close the thin gate, occluding the substrate-binding site from extracellular solution. For Mhp1, the binding of substrate involves the inward bending of the N-terminal half of TM10. Thus the thin gate opens and closes around the substrate-binding pocket upon substrate binding or unbinding, defining the transitions from  $T^{\text{out}}$  to  $T^{\text{M}^{\text{out}}}$  or from  $T^{\text{M}^{\text{in}}}$  to  $T^{\text{in}}$  states.

In contrast to the local changes associated with substrate binding, the isomerization between the outward-facing ( $T^{\text{M}^{\text{out}}}$ ) and inward-facing ( $T^{\text{M}^{\text{in}}}$ ) states involves larger-scale conformational changes spread throughout the transporter. These conformational changes can be conceptualized by applying the two-fold axis of internal pseudo-symmetry to the key transmembrane helices TM1 and TM6, which deviate from this symmetry<sup>25,60</sup>. Rotation of TM1 and TM6 of LeuT about the internal symmetry axis generates an inward-facing model in which the extracellular gate is closed and the intracellular gate is open<sup>60</sup>. Based on this model, it was suggested that the bundle of TM1, TM2, TM6 and TM7 moves as a rigid body in a rocker-switch-like mechanism to alternately open and close the extracellular and intracellular gates<sup>60</sup>. However, this simplification is not consistent with the structural comparisons of the LeuT–Leu and LeuT–Trp complexes or of the Mhp1–apo and substrate-bound states, which indicate that, for example, TM1 is not a rigid body and that there is some degree of independent movement within the helix bundle. Further experimental and computational studies are required to understand the movements that describe this conformational change.

Nevertheless, comparison of the LeuT–Leu (outward-facing,  $T^{\text{M}^{\text{out}}}$ ) and vSGLT–Gal (inward-facing,  $T^{\text{M}^{\text{in}}}$ ) structures suggests that the differences between these states can be described by a reorientation of TM1 and TM6 (TM2 and TM7 in vSGLT), together with movement and bending of TM2 and TM7 (TM3 and TM8 in vSGLT). In the outward-facing state, near the extracellular opening in LeuT, TM1 is about 17 Å and 18 Å away from TM3 and TM10, respectively (Fig. 5a, c) compared with just 7 Å and 5 Å for the equivalent elements in vSGLT (Fig. 5b, d). Similarly, the intracellular cavity is open in vSGLT about 16 Å, measured between TM9 and TM7 (Fig. 5b, f), whereas the same elements in LeuT (TM6 and TM8), with the thick intracellular gate closed, are about 9 Å apart (Fig. 5a, e). The similar magnitude to which the extracellular cavity of LeuT collapses to form the thick gate seen in vSGLT, and to which the thick intracellular gate of LeuT opens to form the cavity in vSGLT, supports the idea that the relationship between the cavities and the thick gates is reciprocally related by the two-fold internal symmetry of the transporter, and that structures of LeuT and

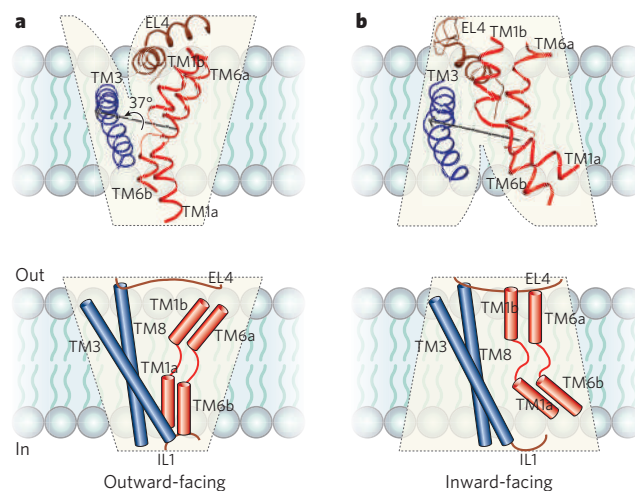


**Figure 6 | Transition between outward-facing and inward-facing states in LeuT-fold transporters.** Transmembrane segments TM1, TM3, TM6 and TM8 line the central translocation pathway, with EL4 and IL1 acting as lids that seal the extracellular and intracellular gates, respectively, in their closed states. **a**, The outward-facing arrangement of central helices in substrate-bound LeuT. **b**, The inward-facing arrangement of central helices in substrate-bound vSGLT. TM8 and IL1 are omitted from the top section for clarity. TM1 and TM6 rotate approximately 37° relative to TM3 and TM8 in transitioning from the outward-facing state adopted by LeuT (**a**) to the inward-facing state adopted by vSGLT (**b**). The rotation axis, shown in black, and the angle of rotation were calculated using DynDom<sup>67</sup>. Cartoon representations of outward-facing and inward-facing states are shown below the corresponding ribbon diagrams. The cartoon representations are adapted, with permission, from ref. 25.

vSGLT largely represent distinct occluded-state ternary intermediates that interconvert during transport. The reorientation of TM1, TM2, TM6 and TM7 (LeuT numbering) between an occluded LeuT-like conformation ( $T^{\text{M}^{\text{out}}}$ ) and an occluded vSGLT-like conformation ( $T^{\text{M}^{\text{in}}}$ ) is therefore likely to approximate the conformational transition that reorients the thin gates of a transporter to the opposite side of the membrane. Additionally, the flexing of TM3 and TM8 may also contribute to the opening and closing of the gates, with these transmembrane helices bending at conserved glycine residues near their midsections, and with IL1, EL4 and the N terminus functioning as flexible flaps, helping to seal the gates in the closed state.

Taken together, the crystal structures of the LeuT fold, namely Mhp1, LeuT and vSGLT, identify two major classes of transition that occur during transport. First, substrate binding and unbinding closes and opens, respectively, the thin gates to occlude or expose the substrate in the primary binding site. Second, the opening and closing of the thick gates switches the transporter between outward-facing and inward-facing states. The opening and closing of the thin gates stem from local conformational changes, some of which involve helix rotations centred on axes that pass through the regions of helical discontinuity. By contrast, the thick-gate transition reorients the occluded substrate-transporter complex by rotating the entire membrane-spanning bundle of helices about a central axis approximately perpendicular to the axis of internal two-fold symmetry (Fig. 6a, b).

How do we know that comparing different transporters in different conformations reliably predicts common mechanistic principles? We don't, but the fact that transporters with the LeuT fold share several common elements of structure and symmetry suggests that basic mechanistic principles are also likely to be shared. However, specific details, related to substrate and transporter interactions and regulation, are likely to differ.

What prevents both gates from opening simultaneously? We suggest that the discontinuous helical regions of TM1 and TM6 provide a hinge around which a small degree of conformational change can occur.

This can be seen in the movements that accompany the binding of the competitive inhibitor tryptophan to LeuT, in which the thin extracellular gate opens by outward movements of TM1b and TM6a. However, TM1 and TM6 are adjacent to TM2 and TM7, and together they form a four-helix bundle. Larger-scale movement of TM1b and TM6a is therefore constrained by TM2 and TM7, perhaps because the latter are continuous  $\alpha$ -helices that lack the non-helical, hinge-like regions present in TM1 and TM6. So substantial outward (opening) movements of TM1b and TM6a, or of TM1a and TM6b, are limited by TM2 and TM7. As a result, both gates may be closed at the same time, but they are prevented from being simultaneously open by the conformational rigidity enforced by TM2 and TM7.

### Future prospects

Recent crystallographic studies of sodium-coupled secondary transporters have greatly advanced our understanding of the structural principles that underlie transporter function. The consistency of these models with the earlier functional studies has allowed us to associate specific conformations with different mechanistic states of the transport cycle. However, this mechanistic description is derived from a patchwork of different transporters fortuitously crystallized in different states. An accurate description of the precise conformational changes that a given transporter undergoes during transport must await further structural, biophysical and computational studies of individual secondary transporters. Additionally, various questions regarding the fundamental nature of the transport cycle remain outstanding. Although it is fairly easy to see how substrate binding leads to the closure of a thin gate, it is harder to deduce the chemical and structural principles that drive the isomerization of the transporter from an outward-facing to an inward-facing state (in other words, open a thick gate). Unlike mechanical models of gating in primary transporters and ion channels, in secondary transporters there is no apparent source of mechanical force to open the thick gate. What structural changes occur in response to the binding of ions? What is the sequence of events that leads to the release of substrate on the cytoplasmic side? How do ions, such as potassium, promote the isomerization of glutamate and serotonin transporters from inward-facing to outward-facing states? Finally, in order to fully understand and appreciate the biological and pharmacological properties unique to human secondary transporters, we will need to solve the crystal structures of eukaryotic homologues. There is clearly much work still to do. ■

- Quick, M. W. (ed.) *Transmembrane Transporters* (Wiley-Liss, 2002).
- Roux, M. J. & Supplisson, S. Neuronal and glial glycine transporters have different stoichiometries. *Neuron* **25**, 373–383 (2000).
- Chakrabarti, A. C. & Deamer, D. W. Permeability of lipid bilayers to amino acids and phosphate. *Biochim. Biophys. Acta* **1111**, 171–177 (1992).
- Supplisson, S. & Roux, M. J. Why glycine transporters have different stoichiometries. *FEBS Lett.* **529**, 93–101 (2002).
- Sobczak, I. & Lolkema, J. S. Structural and mechanistic diversity of secondary transporters. *Curr. Opin. Microbiol.* **8**, 161–167 (2005).
- Wright, E. M. & Turk, E. The sodium/glucose cotransport family SLC5. *Pflügers Arch.* **447**, 510–518 (2004).
- Hebert, S. C., Mount, D. B. & Gamba, G. Molecular physiology of cation-coupled Cl<sup>-</sup> cotransport: the SLC12 family. *Pflügers Arch.* **447**, 580–593 (2004).
- Sonders, M. S., Quick, M. & Javitch, J. A. How did the neurotransmitter cross the bilayer? A closer view. *Curr. Opin. Neurobiol.* **15**, 296–304 (2005).
- Gamba, G. Molecular physiology and pathophysiology of electroneutral cation-chloride cotransporters. *Physiol. Rev.* **85**, 423–493 (2005).
- Murphy, D. L., Lerner, A., Rudnick, G. & Lesch, K. P. Serotonin transporter: gene, genetic disorders, and pharmacogenetics. *Mol. Interv.* **4**, 109–123 (2004).
- Busch, W. & Saier, M. H. Jr The transporter classification (TC) system, 2002. *Crit. Rev. Biochem. Mol. Biol.* **37**, 287–337 (2002).
- Hediger, M. A. et al. The ABCs of solute carriers: physiological, pathological and therapeutic implications of human membrane transport proteins. *Pflügers Arch.* **447**, 465–468 (2004).
- Saier, M. H. Jr A functional-phylogenetic classification system for transmembrane solute transporters. *Microbiol. Mol. Biol. Rev.* **64**, 354–411 (2000).
- Saier, M. H. Jr, Tran, C. V. & Barabote, R. D. TCDB: The Transporter Classification Database for membrane transport protein analyses and information. *Nucleic Acids Res.* **34**, D181–D186 (2006).
- References 11, 13 and 14 provide a comprehensive classification system for membrane transport proteins that includes ion channels as well as primary and secondary transporters.
- Mitchell, P. A general theory of membrane transport from studies of bacteria. *Nature* **180**, 134–136 (1957).
- Mitchell, P. in *Advances in Enzymology and Related Areas of Molecular Biology* (ed. Nord, F. F.) 33–87 (Interscience, 1967).
- Patlak, C. S. Contributions to the theory of active transport: II. The gate type non-carrier mechanism and generalizations concerning tracer flow, efficiency, and measurement of energy expenditure. *Bull. Math. Biophys.* **19**, 209–235 (1957).
- Vidaver, G. A. Inhibition of parallel flux and augmentation of counter flux shown by transport models not involving a mobile carrier. *J. Theor. Biol.* **10**, 301–306 (1966).
- Jardetzky, O. Simple allosteric model for membrane pumps. *Nature* **211**, 969–970 (1966).
- Murakami, S., Nakashima, R., Yamashita, E. & Yamaguchi, A. Crystal structure of bacterial multidrug efflux transporter AcrB. *Nature* **419**, 587–593 (2002).
- Huang, Y., Lemieux, M. J., Song, J., Auer, M. & Wang, D. N. Structure and mechanism of the glycerol-3-phosphate transporter from *Escherichia coli*. *Science* **301**, 616–620 (2003).
- Abramson, J. et al. Structure and mechanism of the lactose permease of *Escherichia coli*. *Science* **301**, 610–615 (2003).
- Yernool, D., Boudker, O., Jin, Y. & Gouaux, E. Structure of a glutamate transporter homologue from *Pyrococcus horikoshii*. *Nature* **431**, 811–818 (2004).
- Hunte, C. et al. Structure of a Na<sup>+</sup>/H<sup>+</sup> antiporter and insights into mechanism of action and regulation by pH. *Nature* **435**, 1197–1202 (2005).
- Yamashita, A., Singh, S. K., Kawate, T., Jin, Y. & Gouaux, E. Crystal structure of a bacterial homologue of Na<sup>+</sup>/Cl<sup>-</sup> dependent neurotransmitter transporters. *Nature* **437**, 215–223 (2005).
- Screpanti, E. & Hunte, C. Discontinuous membrane helices in transport proteins and their correlation with function. *J. Struct. Biol.* **159**, 261–267 (2007).
- Faham, S. et al. The crystal structure of a sodium galactose transporter reveals mechanistic insights into Na<sup>+</sup>/sugar symport. *Science* **321**, 810–814 (2008).
- Weyand, S. et al. Structure and molecular mechanism of a nucleobase-cation-symport-1 family transporter. *Science* **322**, 709–713 (2008).
- Wright, E. M., Loo, D. D. F., Hirayama, B. A. & Turk, E. Surprising versatility of Na<sup>+</sup>-glucose cotransporters: SLC5. *Physiology* **19**, 370–376 (2004).
- Chen, N. H., Reith, M. E. & Quick, M. W. Synaptic uptake and beyond: the sodium- and chloride-dependent neurotransmitter transporter family SLC6. *Pflügers Arch.* **447**, 519–531 (2004).
- Barker, E. L., Moore, K. R., Rakhshan, F. & Blakely, R. D. Transmembrane domain I contributes to the permeation pathway for serotonin and ions in the serotonin transporter. *J. Neurosci.* **19**, 4705–4717 (1999).
- Rudnick, G. Serotonin transporters — structure and function. *J. Membr. Biol.* **213**, 101–110 (2006).
- Kanner, B. I. & Zomot, E. Sodium-coupled neurotransmitter transporters. *Chem. Rev.* **108**, 1654–1668 (2008).
- Ben-Yona, A. & Kanner, B. I. Transmembrane domain 8 of the  $\gamma$ -aminobutyric acid transporter GAT-1 lines a cytoplasmic accessibility pathway into its binding pocket. *J. Biol. Chem.* **284**, 9727–9732 (2009).
- Slotboom, D. J., Lolkema, J. S. & Konings, W. N. Membrane topology of the C-terminal half of the neuronal, glial, and bacterial glutamate transporter family. *J. Biol. Chem.* **271**, 31317–31321 (1996).
- Grunewald, M., Bendahan, A. & Kanner, B. I. Biotinylation of single cysteine mutants of the glutamate transporter GLT-1 from rat brain reveals its unusual topology. *Neuron* **21**, 623–632 (1998).
- Seal, R. P. & Amara, S. G. A reentrant loop domain in the glutamate carrier EAAT1 participates in substrate binding and translocation. *Neuron* **21**, 1487–1498 (1998).
- Toyoshima, C., Nakasako, M., Nomura, H. & Ogawa, H. Crystal structure of the calcium pump of sarcoplasmic reticulum at 2.6 Å resolution. *Nature* **405**, 647–655 (2000).
- Dutzler, R., Campbell, E. B., Cadene, M., Chait, B. T. & MacKinnon, R. X-ray structure of a Cl<sup>-</sup> channel at 3.0 Å reveals the molecular basis of anion selectivity. *Nature* **415**, 287–294 (2002).
- Singh, S. K., Piscitelli, C. L., Yamashita, A. & Gouaux, E. A competitive inhibitor traps LeuT in an open-to-out conformation. *Science* **322**, 1655–1661 (2008).

This paper provides a crystallographic and functional analysis of LeuT with several different ligands that correlates the occluded state to transportable ligands and identifies a tryptophan as a competitive inhibitor that traps an open-to-out conformation.

Shi, L., Quick, M., Zhao, Y., Weinstein, H. & Javitch, J. A. The mechanism of a neurotransmitter:sodium symporter-inward release of Na<sup>+</sup> and substrate is triggered by a substrate in a second binding site. *Mol. Cell* **30**, 667–677 (2008).

Celik, L., Schiott, B. & Tajkhorshid, E. Substrate binding and formation of an occluded state in the leucine transporter. *Biophys. J.* **94**, 1600–1612 (2008).

Hilger, D., Bohm, M., Hackmann, A. & Jung, H. Role of Ser-340 and Thr-341 in transmembrane domain IX of the Na<sup>+</sup>/proline transporter PutP of *Escherichia coli* in ligand binding and transport. *J. Biol. Chem.* **283**, 4921–4929 (2008).

De La Vieja, A., Reed, M. D., Ginter, C. S. & Carrasco, N. Amino acid residues in transmembrane segment IX of the Na<sup>+</sup>/I<sup>-</sup> symporter play a role in its Na<sup>+</sup> dependence and are critical for transport activity. *J. Biol. Chem.* **282**, 25290–25298 (2007).

The mutation of conserved serine and threonine residues in TM9 of the NIS transporter (SSS family) shows that they are involved in Na<sup>+</sup> binding and translocation.

Zhou, Y., Zomot, E. & Kanner, B. I. Identification of a lithium interaction site in the GABA transporter GAT-1. *J. Biol. Chem.* **281**, 22092–22099 (2006).

Noskov, S. Y. & Roux, B. Control of ion selectivity in LeuT: two Na<sup>+</sup> binding sites with two different mechanisms. *J. Mol. Biol.* **377**, 804–818 (2008).

Caplan, D. A., Subbotina, J. O. & Noskov, S. Y. Molecular mechanism of ion-ion and ion-substrate coupling in the Na<sup>+</sup>-dependent leucine transporter LeuT. *Biophys. J.* **95**, 4613–4621 (2008).

Talvenheimo, J., Fishkes, H., Nelson, P. J. & Rudnick, G. The serotonin transporter-imipramine “receptor”. *J. Biol. Chem.* **258**, 6115–6119 (1983).

Gu, H. H., Wall, S. & Rudnick, G. Ion coupling stoichiometry for the norepinephrine transporter in membrane vesicles from stably transfected cells. *J. Biol. Chem.* **271**, 6911–6916 (1996).

Keynan, S. & Kanner, B. I.  $\gamma$ -Aminobutyric acid transport in reconstituted preparations from rat brain: coupled sodium and chloride fluxes. *Biochemistry* **27**, 12–17 (1988).

51. Diez-Sampedro, A., Eskandari, S., Wright, E. M. & Hirayama, B. A. Na<sup>+</sup>-to-sugar stoichiometry of SGLT3. *Am. J. Physiol. Renal Physiol.* **280**, F278–F282 (2001).
52. Mackenzie, B., Loo, D. D. F. & Wright, E. M. Relationships between Na<sup>+</sup>/glucose cotransporter (SGLT1) currents and fluxes. *J. Membr. Biol.* **162**, 101–106 (1998).
53. Eskandari, S. *et al.* Thyroid Na<sup>+</sup>/I<sup>-</sup> symporter. Mechanism, stoichiometry, and specificity. *J. Biol. Chem.* **272**, 27230–27238 (1997).
54. Forrest, L. R., Tavoulari, S., Zhang, Y. W., Rudnick, G. & Honig, G. Identification of a chloride ion binding site in Na<sup>+</sup>/Cl<sup>-</sup>-dependent transporters. *Proc. Natl Acad. Sci. USA* **104**, 12761–12766 (2007).
55. Zomot, E. *et al.* Mechanism of chloride interaction with neurotransmitter:sodium symporters. *Nature* **449**, 726–730 (2007).
56. Singh, S., Yamashita, A. & Gouaux, E. Antidepressant binding site in a bacterial homologue of neurotransmitter transporters. *Nature* **448**, 952–956 (2007).  
**This paper presents a structural concept for the non-competitive inhibition of NSS transporters by tricyclic antidepressants.**
57. Boudker, O., Ryan, R., Yernool, D., Shimamoto, K. & Gouaux, E. Coupling substrate and ion binding to extracellular gate of a sodium-dependent aspartate transporter. *Nature* **445**, 387–393 (2007).
58. Kavanaugh, M. P., Bendahan, A., Zerangue, N., Zhang, Y. & Kanner, B. I. Mutation of an amino acid residue influencing potassium coupling in the glutamate transporter GLT-1 induces obligate exchange. *J. Biol. Chem.* **272**, 1703–1708 (1997).
59. Keyes, S. R. & Rudnick, G. Coupling of transmembrane proton gradients to platelet serotonin transport. *J. Biol. Chem.* **257**, 1172–1176 (1982).
60. Forrest, L. R. *et al.* Mechanism for alternating access in neurotransmitter transporters. *Proc. Natl Acad. Sci. USA* **105**, 10338–10343 (2008).  
**This paper proposes a model for an inward-facing conformation of LeuT based on the structure of outward-facing LeuT-Leu and the inverted structural pseudo-symmetry.**
61. Jacobs, M. T., Zhang, Y. W., Campbell, S. D. & Rudnick, G. Ibogaine, a noncompetitive inhibitor of serotonin transport, acts by stabilizing the cytoplasm-facing state of the transporter. *J. Biol. Chem.* **282**, 29441–29447 (2007).
62. Zhang, Y.-W. & Rudnick, G. The cytoplasmic substrate permeation pathway of serotonin transporter. *J. Biol. Chem.* **281**, 36213–36220 (2006).
63. Zhang, Y. W. & Rudnick, G. Cysteine-scanning mutagenesis of serotonin transporter intracellular loop 2 suggests an  $\alpha$ -helical conformation. *J. Biol. Chem.* **280**, 30807–30813 (2005).
64. Zhou, Z. *et al.* LeuT-desipramine structure reveals how antidepressants block neurotransmitter uptake. *Science* **317**, 1390–1393 (2007).
65. Apparsundaram, S., Stockdale, D. J., Henningsen, R. A., Milla, M. E. & Martin, R. S. Antidepressants targeting the serotonin reuptake transporter act via a competitive mechanism. *J. Pharmacol. Exp. Ther.* **327**, 982–990 (2008).
66. Hirayama, B. A., Diez-Sampedro, A. & Wright, E. M. Common mechanisms of inhibition for the Na<sup>+</sup>/glucose (hSGLT1) and Na<sup>+</sup>/Cl<sup>-</sup>/GABA (hGAT1) cotransporters. *Br. J. Pharmacol.* **134**, 484–495 (2001).  
**This paper demonstrates a common principle for inhibition between two functionally unrelated families that hints at the underlying structural conservation.**
67. Hayward, S. & Berendsen, H. J. Systematic analysis of domain motions in proteins from conformational change: new results on citrate synthase and T4 lysozyme. *Proteins* **30**, 144–154 (1998).

**Acknowledgements** This work was supported by the US National Institutes of Health. E.G. is an investigator with the Howard Hughes Medical Institute. We thank R. Hibbs, K. Hollenstein, H. Owen, S. Singh and A. Sobolevsky for helpful comments and L. Vaskalis for assistance with the figures.

**Author Information** Reprints and permissions information is available at [www.nature.com/reprints](http://www.nature.com/reprints). The authors declare no competing financial interests. Correspondence should be addressed to E.G. ([gouauxe@ohsu.edu](mailto:gouauxe@ohsu.edu)).